Cancer Management and Research

Elevate Series

Open Access Full Text Article

ORIGINAL RESEARCH

Distinct Lung Adenocarcinoma-Associated Microbiota Are Associated with Inflammatory Immune Landscapes and Tumor Cell Proliferation via LCIIAR–ISG15 Regulatory Networks

Shipu Liu[1], Zijian Zhang[2]

[1]Department of Occupational Medicine and Clinical Toxicology, Beijing Chaoyang Hospital, Capital Medical University, Beijing, 100020, People's Republic of China; [2]Department of Urology, Beijing Chaoyang Hospital, Capital Medical University, Beijing, 100020, People's Republic of China

Correspondence: Zijian Zhang, Department of Urology, Beijing Chaoyang Hospital, Capital Medical University, Beijing, People's Republic of China, Email zzhang742@uwalumni.com

Introduction: Emerging research emphasizes the critical role of local microbiota in shaping the tumor microenvironment (TME) and influencing cancer progression. Lung adenocarcinoma (LUAD) is distinguished by unique bacterial communities that appear to regulate immune responses, gene expression, and patient outcomes.

Methods: We compiled microbiome profiles from several cancer types—including LUAD, lung squamous cell carcinoma (LUSC), breast carcinoma (BRCA), and thyroid carcinoma (THCA)—using public databases. Non-negative matrix factorization (NMF) was employed to categorize LUAD cases based on TME features, while DESeq2 was used to pinpoint bacterial taxa with differing abundance. Multi-omics networks were developed to integrate microbial, transcriptomic, and clinical data. For in vitro verification, we conducted siRNA-mediated knockdown of the long non-coding RNA LCIIAR and ISG15 in Lewis lung carcinoma cells, followed by proliferation assays.

Results: In contrast to LUSC, BRCA, and THCA, LUAD exhibited distinct microbial populations, with notable enrichment of Cylindrospermopsis, Cyanothece, and Sulfolobus. NMF clustering identified two LUAD subtypes with differing prognoses. One longer survival cluster, marked by reduced bacterial presence and stronger antitumor immunity—reflected in stronger immune response, increased effector T cells activity, and greater immune cell infiltration. A competing endogenous RNA (ceRNA) network analysis established a link between LCIIAR and ISG15, both overexpressed in LUAD and associated with worse survival outcomes. Knockdown LCIIAR or ISG15 through siRNA significantly inhibited lung cancer cell proliferation, pointing to their roles in tumor growth and ceRNA-mediated regulation.

Conclusion: LUAD features a distinctive microbiota that engages with inflammatory and ceRNA regulatory pathways. These observations underscore the value of targeting microbiome-influenced mechanisms, such as the LCIIAR–ISG15 axis, as a promising approach to enhance treatment outcomes in lung adenocarcinoma.

Keywords: lung adenocarcinoma, microbiota, tumor microenvironment, ceRNA network

Introduction

The connection between cancer and microbial agents has undergone significant evolution in understanding over centuries. Symbiotic microbiota residing within the human body can affect metabolic pathways, growth dynamics, and neoplastic cell functions, thereby impacting the tumor microenvironment.[1] A comprehensive global analysis estimated that in 2018, around 13% of all cancer cases were linked to infectious agents, including viruses, bacteria, and parasites.[2] Bacteria are increasingly acknowledged for their contributions to the onset of various cancers and their influence on responses to treatments, such as immune checkpoint inhibitors.[3,4] This deepening insight highlights the microbiome's potential to advance diagnostic and therapeutic strategies.[5,6]

Dysbiosis, defined as an imbalance in microbial communities, is implicated in cancer development and progression through processes such as mutagenesis, epigenetic alterations, and immune modulation.[7] For example, Fusobacterium

Received: 4 February 2025
Accepted: 29 June 2025
Published: 4 July 2025

nucleatum manipulates glucose metabolism to support colorectal cancer development,[8] while other bacteria adjust immune responses and affect tumor prognosis.[9] Strikingly, a randomized controlled trial showed that fecal microbiota transplantation could reverse resistance to immune checkpoint inhibitors in patients with treatment-resistant melanoma, reinforcing the pivotal role of commensal bacteria in tumor immunity.[10]

Multiple microbial niches exist within the human body, particularly at barrier surfaces. The interplay between these microbiota and tumor progression, such as the relationship between the gut microbiome and colorectal cancer, has been extensively studied.[11] However, these microbial sites have lower biomass than the gastrointestinal tract, and their roles in tumorigenesis are still being explored. The lungs, in particular, are exposed to local inflammation from infectious exposures, environmental allergens, pollutants, and cigarette smoke. Non-small cell lung cancer (NSCLC), the most common type of lung cancer, is the leading cause of cancer-related deaths globally. Understanding the factors contributing to its development and treatment response is crucial for public health.[12] In NSCLC tissues, exposing airway epithelial cells to specific bacterial taxa such as Prevotella, Streptococcus, and Veillonella activates the PI3K and AKT signaling pathways, correlating with oncogenic transcriptome programs.[13] Lung adenocarcinoma (LUAD), a major subtype of NSCLC, comprises approximately 40% of lung cancer cases and presents a poor prognosis, contributing significantly to the lung cancer burden.[14] Recent studies have found that depleting the microbiota in a mouse model of lung adenocarcinoma with Kras mutation and p53 deletion significantly suppressed tumor growth.[15]

The precise influence of the lung microbiome on NSCLC remains poorly defined, partly because isolating viable microbial cells from healthy lung tissue is challenging due to low biomass or technical limitations.[16] Chronic inflammation stands out as a key risk factor for NSCLC, underscoring the need for detailed mechanistic studies to clarify the microbiota's role in cancer initiation and progression. Recent efforts analyzing whole-genome sequencing and transcriptomic data from The Cancer Genome Atlas (TCGA) with the SHOGUN algorithm have estimated commensal bacterial abundance across a wide array of tumor samples, offering a valuable means to investigate microbial roles in specific tumor contexts.[17]

This study aims to outline differences in microbial composition across various cancers, with a particular focus on lung adenocarcinoma. By examining how these microbial populations shape the oncogenic landscape, we aim to discover new possibilities for targeted therapeutic interventions.

Materials and Methods

Data Collection

Microbial composition data for lung adenocarcinoma (LUAD), lung squamous cell carcinoma (LUSC), breast carcinoma (BRCA), and thyroid carcinoma (THCA) were sourced from the Cancer Microbiome database (http://cancermicrobiome.ucsd.edu/CancerMicrobiome_DataBrowser).[17] Tumor mutational burden (TMB), immunophenoscore (IPS), and T-cell and B-cell receptor repertoire profiles were obtained from MF Portrait by BostonGene (https://science.bostongene.com/tumor-portrait).[18] Multiple viral signatures for LUAD were derived using the VirusScan pipeline, with a threshold of 100 reads applied to determine positive or negative status.[19] Additional datasets, including gene expression, miRNA profiles, DNA copy number variation (CNV), methylation, ATAC-seq peak-calling, and clinical data, were retrieved from UCSC Xena (https://xenabrowser.net/datapages).

Microbiome Data Analysis

Microbial abundance data from the Cancer Microbiome database were aligned with clinical data from UCSC Xena using sample identifiers. To minimize batch effects, microbial abundance data derived from RNA-seq were selected, encompassing both tumor tissue and adjacent normal solid tissue. These data were normalized to reads per million (RPM). Alpha diversity was assessed using the Shannon index, and beta diversity was evaluated with Bray-Curtis distances, both calculated using the "vegan" R package (v2.6.4).[20] Principal coordinates analysis (PCoA) was performed to visualize microbial community differences.[21] Variations in microbial communities were tested using PERMANOVA and Mantel tests. Differentially abundant species were identified with the "DESeq2" package (v3.19), applying an adjusted P-value threshold of 0.05.[22]

TME Signature and NMF-Based Clustering Analysis

Tumor microenvironment (TME) signatures for LUAD samples (n = 477) were acquired from BostonGene and normalized using median scaling. These signatures underwent non-negative matrix factorization (NMF) clustering (v0.27) with K-means, testing cluster numbers from 1 to 5.[23] Two distinct clusters were selected based on cophenetic, dispersion, and silhouette scores. Survival analysis between these TME clusters was conducted using the "survival" package (v3.6.4) in R.

Network Analysis

Interaction networks incorporating TME features, immune checkpoints, viral abundance, and differentially abundant species were constructed using Spearman correlation analysis. The STRING database (https://string-db.org/) was employed to investigate potential interactions among differentially expressed genes (DEGs), generating protein interaction networks to illustrate regulatory relationships.[24] The MCODE algorithm was applied to detect densely connected regions within these networks.[25] Network co-presence and exclusivity were evaluated using Cytoscape's Network Analyzer tool (v3.10.1).[26]

ceRNA Network Analysis

The GDCRNATools pipeline (v1.24.0) was used to examine the lncRNA–mRNA competing endogenous RNA (ceRNA) network in LUAD TME clusters, based on expression data for 187 lncRNAs, miRNAs, and mRNAs.[27] The analysis targeted key genes, including BRAF and ISG15. Data were preprocessed, normalized, and analyzed with default parameters (Pearson's $r > 0.4$, $P < 0.05$). Interactions were validated using the ENCORI platform. Priority was given to interactions exhibiting differential expression across TME clusters, high expression levels, and support from prior literature, such as the LCIIAR–miRNA–ISG15 axis. Databases such as miRBase v22 and starBase v2.0 were utilized to ensure robust and accurate network construction.

Web Resource Integration Archives

The gene mutation and expression profiles of immune-related genes in LUAD were analyzed using cBioPortal (https://www.cbioportal.org/). Survival analysis for ISG15 and LCIIAR was performed with the LnCeCell database (http://bio-bigdata.hrbmu.edu.cn/LnCeCell/).[28] The multi-omics landscape for ISG15 was explored using UCSC Xena, incorporating the GDC Pan-Cancer (PANCAN) database (n = 323), TCGA LUAD database, and TCGA LUSC database (n = 37). Survival analysis was conducted using the median as the cutoff point.

siRNA-Mediated Gene Knockdown and Quantitative PCR Analysis

Small interfering RNAs (siRNAs) targeting LCIIAR and ISG15 were designed and synthesized using BLOCK-iT RNAi Designer (Thermo Fisher Scientific, Carlsbad, CA). Lewis lung carcinoma cells were transfected with these siRNAs using Lipofectamine 3000 (L3000015, Invitrogen, Carlsbad, CA) according to the manufacturer's instructions. After 24 hours, total RNA was extracted using an RNA isolation kit (RC101-01, Vazyme, Nanjing, China). cDNA was synthesized from 1 μg of total RNA with a reverse transcription kit (R223-01, Vazyme). Quantitative real-time PCR (qPCR) was conducted to measure LCIIAR and ISG15 expression using gene-specific primers and SYBR Green PCR Master Mix (Q711-02, Vazyme). Expression levels were normalized to the housekeeping gene GAPDH. Experiments were performed in triplicate, and relative expression levels were calculated using the 2^–ΔΔCt method (see Table S1 for sequences).

Luciferase Assay

To investigate the mechanism by which LCIIAR regulates ISG15 protein expression, a luciferase reporter plasmid (Figure S1) was constructed, connecting the CDS and 3′ UTR of ISG15 to luciferase mRNA. This plasmid was co-transfected with either an LCIIAR overexpression plasmid, miR-22-3p and miR-3127-5p mimics, or inhibitors. Luciferase activity was measured 48 hours post-transfection using the Luciferase Assay System (DD1203-03, Vazyme). The miRNA scramble, miR-22-3p mimic, miR-22-3p inhibitor, miR-3127-5p mimic, and miR-3127-5p inhibitor were sourced from RIBOBIO Corporation (Guangzhou, China).

Cell Proliferation Assay Using CCK-8

To assess the effects of LCIIAR or ISG15 knockdown on cell proliferation, a Cell Counting Kit-8 (CCK-8, A311-01, Vazyme) assay was conducted. Lewis lung carcinoma cells (LL/2 (LLC1), ATCC number CRL-1642) were cultured, frozen, and revived in our laboratory. Following transfection with siRNAs targeting LCIIAR or ISG15, cells were seeded into 96-well plates at a density of 5 × 10^3 cells per well. Cell proliferation was measured at 24, 48, and 72 hours post-transfection. At each time point, 10 μL of CCK-8 solution was added to each well, and plates were incubated at 37°C for 2 hours. Absorbance was recorded at 450 nm using a microplate reader.

Statistical Analysis

Statistical comparisons between two groups were performed using the Wilcoxon rank sum test. Linear associations between variables were evaluated with Spearman correlation analysis. Alpha diversity was assessed using the Mann–Whitney test, and principal coordinates analysis (PCoA) was visualized with Bray-Curtis distances. Variations in microbial compositions were tested using PERMANOVA or the Mantel test. Survival analyses were conducted with Log rank tests, and Cox regression was applied for multivariate analysis. Experimental data were analyzed using one-way ANOVA, with $P < 0.05$ considered statistically significant. The Benjamini-Hochberg method was used to control the false discovery rate in multiple testing scenarios. All statistical analyses were performed in R (v4.4.0).

Results

Distinct Microbial Diversity and Composition Across Cancer Types

We analyzed microbial characteristics in patients with lung adenocarcinoma (LUAD, n=528), lung squamous cell carcinoma (LUSC, n=442), breast carcinoma (BRCA, n=1166), and thyroid carcinoma (THCA, n=186) using the Cancer Microbiome "SHOGUN" RNA-seq dataset. These cancers encompassed those potentially exposed to the external environment (LUAD and LUSC) and contrast tumors not directly associated with lung microbiota (BRCA and THCA). At the phylum level, identified bacterial sequences predominantly belonged to Actinobacteria, Bacteroidetes, Candidatus, Chlamydiae, Firmicutes, and Proteobacteria. Notably, lung tumors (LUAD and LUSC) exhibited greater abundance of these bacterial phyla compared to BRCA and THCA (Figure 1A).

In LUAD tissues, bacterial counts differed significantly between primary tumor (PT) and solid tissue normal (STN) samples, with the latter serving as controls (Figure 1B). However, no significant differences in Shannon index values were observed among the cancer types (Figure 1C). Beta diversity analysis, based on Bray-Curtis principal coordinates analysis (PCoA), revealed distinct clustering differences in the microbiota across the four cancer types (Figure 1D). PERMANOVA confirmed significant beta diversity differences between LUAD and LUSC ($P<0.001$ and $P=0.032$, respectively), indicating distinct microbial communities in lung cancers (Figure 1E).

The volcano plots indicated differentially abundant bacterial genera between PT and STN tissues. In lung cancers, genera such as Cyanothece, Sulfolobus, and Alcanivorax were enriched, with Cylindrospermopsis specifically enriched in LUAD. Although Cylindrospermopsis showed higher abundance in LUAD tumor tissues than in normal tissues, its relative abundance varied across tumor subtypes, suggesting its role may depend on the tumor microenvironment and molecular subtype. In contrast, Lachnoclostridium and Ralstonia were enriched in BRCA and THCA, respectively (Figure 1F). Venn diagrams illustrated the overlap of differentially abundant genera between PT and STN across cancer types, revealing eight genera shared between the two lung cancers but fewer shared with non-lung cancers (Figure S2).

Immune Clustering Distinguishes Prognosis in LUAD

We investigated the associations between microbial diversity, composition, and both clinical and immune characteristics in tumor tissues. Analyzed variables included gender, stage, tumor mutational burden (TMB), molecular functional portrait (MFP) signature, and immune features such as immune subtype, immune cell infiltration score (IPS). In LUAD, bacterial read counts and diversity correlated significantly with several clinical and immune characteristics, notably the Shannon indices of BCR and TCR, T and N stages, and tumor purity (Figure 2A). Specifically, we observed significant differences in the Shannon index across different T stages, and significant differences in microbial community structure

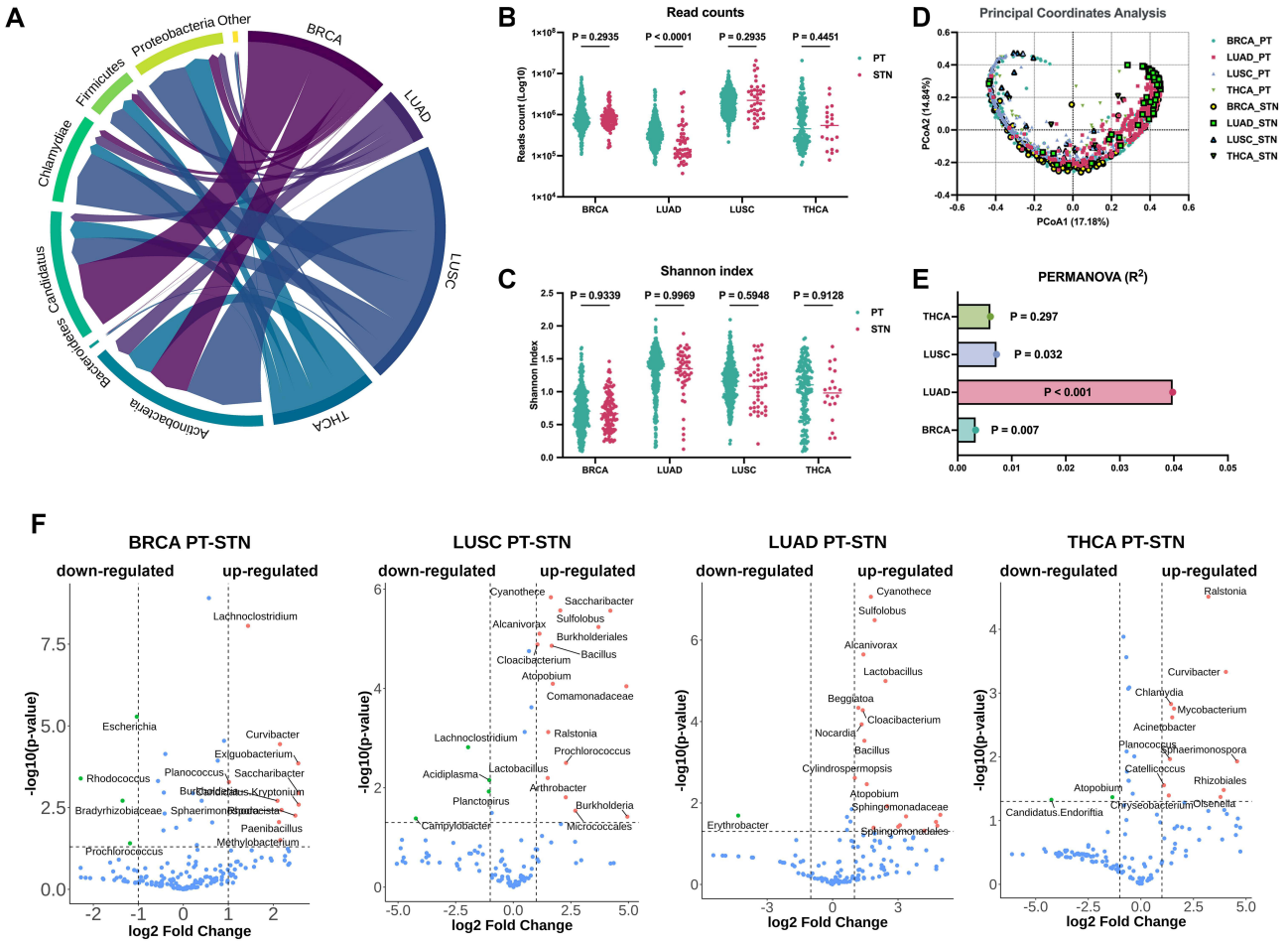

Figure 1 Distinct microbiome diversity and composition across various tumor types. (**A**) High-abundance bacterial sequences at the phylum level were analyzed in primary tumors (PT) and normal solid tissues (STN) from lung adenocarcinoma (LUAD), lung squamous cell carcinoma (LUSC), and control tumors not directly associated with the lung microbiota, including breast carcinoma (BRCA) and thyroid carcinoma (THCA). The distribution of sequence reads for six representative bacterial taxa is presented. (**B**) Bacterial sequence counts and (**C**) Shannon diversity indices were compared between PT and STN using Mann–Whitney test. (**D**) Principal coordinates analysis (PCoA) of Bray-Curtis distances calculated from bacterial sequence reads in PT and STN; each point represents a sample. (**E**) Differences in bacterial β-diversity among tumor samples were evaluated using PERMANOVA. (**F**) Volcano plot illustrating differences in bacterial abundance between each PT and the corresponding STN, identified using DESeq2 analysis. Upregulated taxa indicate enrichment in tumors ($|Log^2FC| > 1$); statistical significance was considered at $P < 0.05$.

across different N stages, as measured by Bray-Curtis distance. These findings suggest a robust association between commensal bacteria and the immunosuppressive microenvironment in LUAD. By contrast, LUSC displayed fewer associations between bacterial flora and immune features.

Using non-negative matrix factorization (NMF) based on tumor microenvironment (TME) signatures, we classified LUAD patients into two clusters (Figure 2B and Table S2). Survival analysis revealed significant differences between these clusters, with Cluster 1 associated with a better prognosis (Figure 2B). Cluster 1 exhibited lower bacterial read counts than Cluster 2 (Figure 2C), though no significant differences in alpha diversity were observed between the clusters (Figure 2C). Beta diversity analysis indicated significant differences between the clusters (PERMANOVA, P=0.037) (Figure 2D). DESeq2 analysis showed that genera such as Cylindrospermopsis and Saccharibacter were enriched in Cluster 1, which correlated with improved prognosis (Figure 2E).

Tumor Commensal Bacteria Correlate with an Inflammatory TME in LUAD

Building on these observations, we further analyzed TME signatures and found that Cluster 1 was characterized by lower proliferation rates and heightened immune responses, including elevated expression of MHC class I molecules, natural

https://doi.org/10.2147/CMAR.S520098

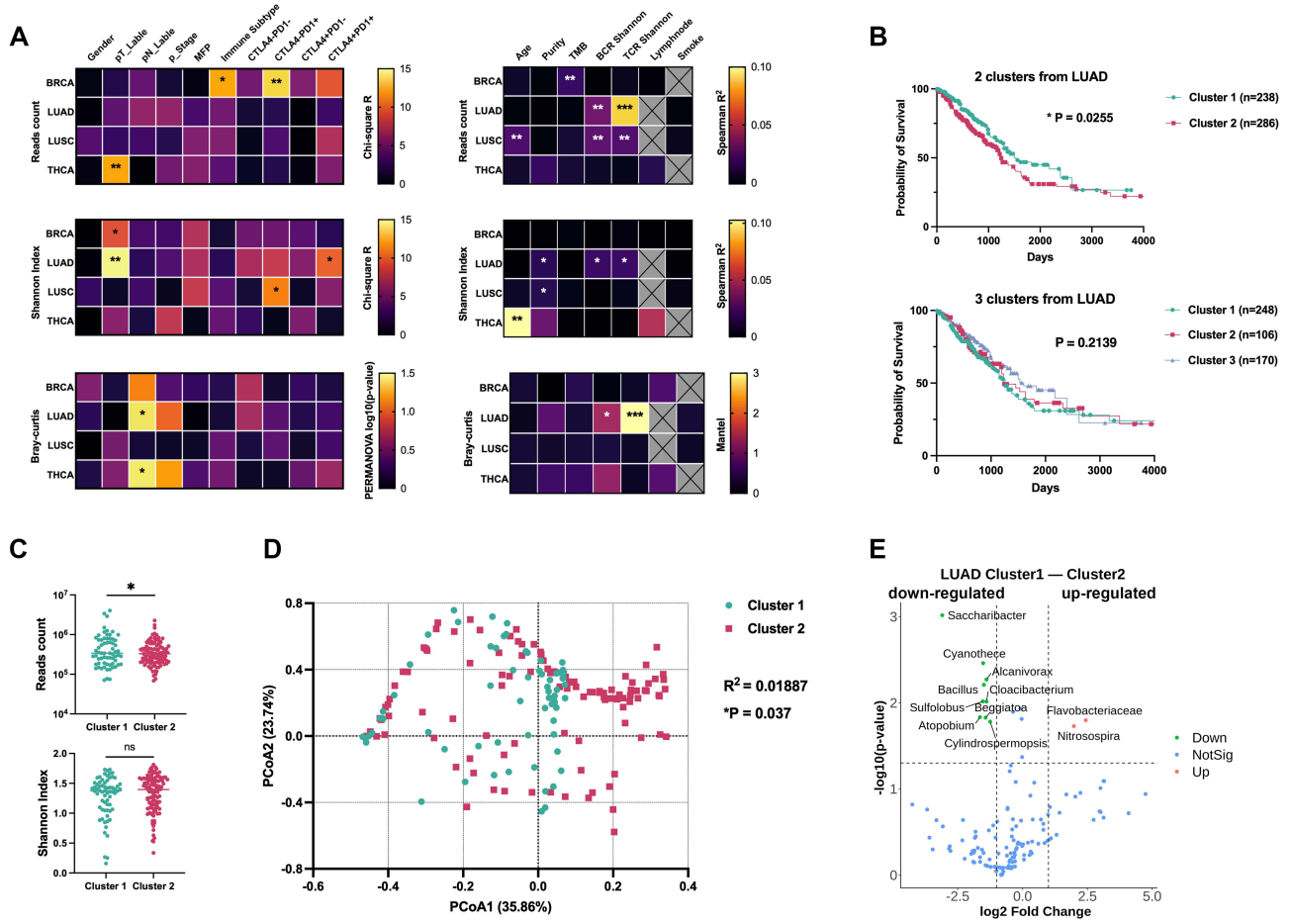

Figure 2 Clustering of immunological features significantly distinguishes LUAD prognosis. (**A**) The left heatmap shows correlations between bacterial sequence reads, Shannon α-diversity index (analyzed by Mann–Whitney test), and Bray-Curtis β-diversity distance (evaluated by PERMANOVA) with tumor and immune-related categorical variables. The right heatmap displays correlations with continuous variables, using Spearman regression for α-diversity and Mantel regression for β-diversity. Statistical significance is indicated by * $P < 0.05$, ** $P < 0.01$, *** $P < 0.001$. (**B**) Kaplan-Meier survival curves showing differences in survival times between groups defined by the non-negative matrix factorization (NMF) algorithm based on tumor immune microenvironment characteristics; significance assessed using the Log rank test. (**C**) Differences in bacterial sequence reads and Shannon α-diversity index between the two groups were analyzed using Student's *t*-test (* $P < 0.05$). (**D**) PCA of Bray-Curtis distances between the two groups; differences in bacterial β-diversity were assessed using PERMANOVA. (**E**) Volcano plot showing differences in bacterial abundance between the groups, identified using DESeq2 analysis. Upregulated taxa indicate enrichment in tumors ($|Log^2FC| > 0.5$); $P < 0.05$ was considered statistically significant.

killer (NK) cells, and effector cells (Figure 3A). Immune checkpoint molecules such as CTLA4, LAG3, CD80, and CD86 were also significantly increased in Cluster 1 (Figure 3B). Immune infiltration analysis using Cibersortx revealed enrichment of pro-inflammatory cells, including effector T cells, in Cluster 1, suggesting a stronger immune response (Figures 3C and S4).

We constructed a multi-omics interaction network incorporating TME features, immune checkpoint genes, viral abundances, and differentially abundant bacterial genera (Figure 3D). Within this network, commensal bacteria such as Sulfolobus, Cylindrospermopsis, and Cyanothece were prominent and strongly correlated with immune microenvironment characteristics, including effector cell presence and NK cell activity. Viral interactions within the network were relatively weak.

Differential gene expression analysis between the clusters identified significant differences in protein-coding genes, pseudogenes (eg, TLK2P2), and non-coding RNAs (eg, TTC3-AS1) (Figure 3E). A protein-protein interaction (PPI) network, constructed from genes enriched in Cluster 2 and analyzed with minimal common oncology data elements (MCODE), identified a core set of interacting genes comprising typical inflammatory factors (Figure 3F). These findings emphasize the pivotal role of the microbiota in immunoregulation in LUAD and indicate that commensal bacterial enrichment is closely tied to inflammatory characteristics within the TME. Given these strong associations between

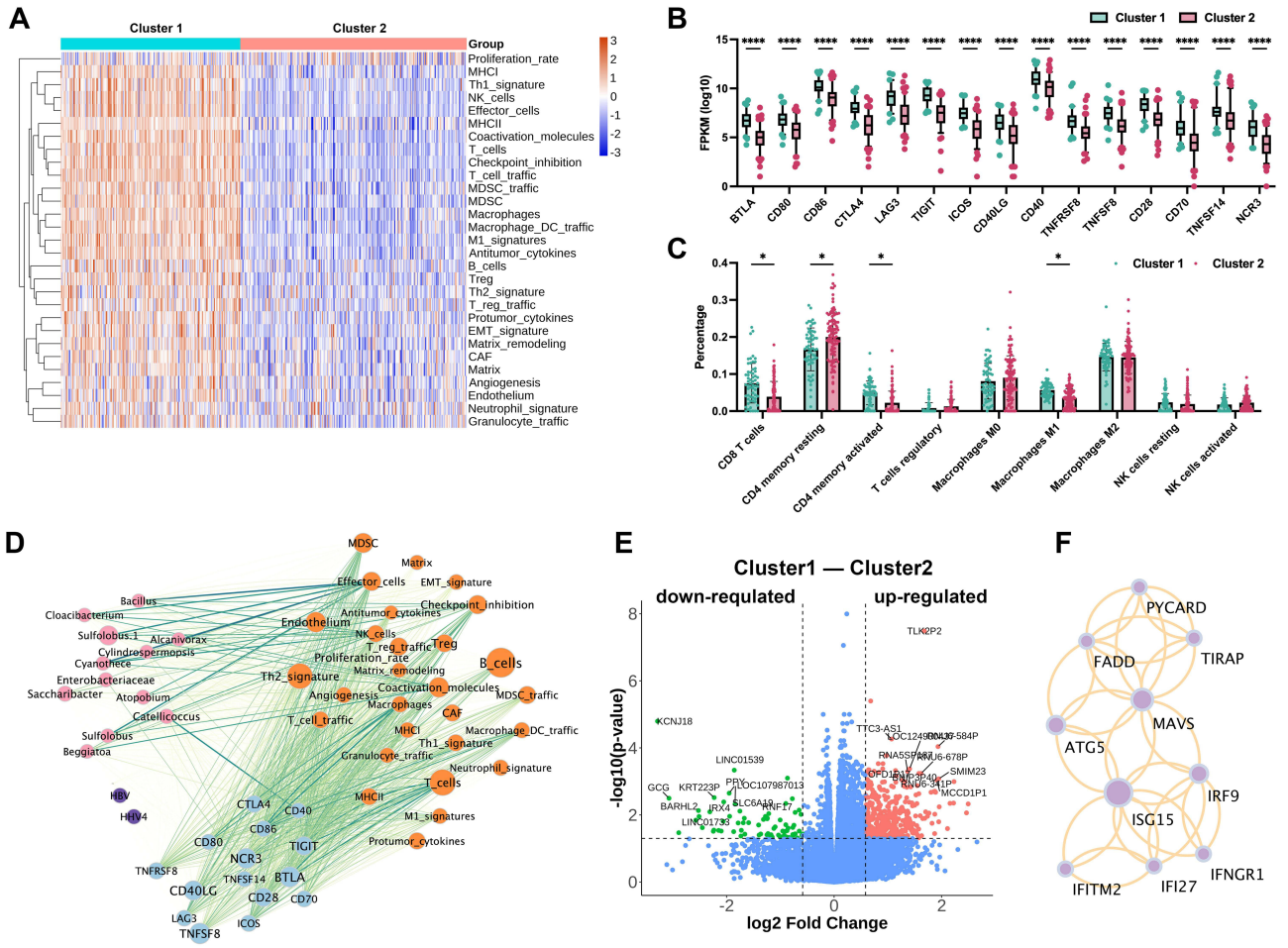

Figure 3 Significant correlations between tumor-associated microbiota, tumor immune microenvironment, and TME signature genes. (**A**) Heatmap displaying clustering of tumor microenvironment (TME) signature genes across different clusters. (**B**) Differential expression of immune checkpoint-related genes between clusters, assessed using Student's *t*-test (**** $P < 0.0001$). (**C**) Immune infiltration analysis by Cibersortx suggests differences in immune cells (* $P < 0.05$). (**D**) Multi-omics interaction network constructed among clusters for TME signature genes, immune checkpoint genes, and viral and bacterial abundances using Spearman correlation analysis, visualized with Cytoscape. Node color indicates type, node size reflects weight, and line color intensity represents interaction strength (intra-group interactions not shown). (**E**) Volcano plot showing differential gene expression between clusters calculated using DESeq2 analysis ($|Log^2FC| > 0.5$); $P < 0.05$ was considered statistically significant. (**F**) Interaction network and clustering of differentially expressed genes between clusters, constructed using STRING and MCODE algorithms.

bacterial presence and inflammatory signaling, we proceeded to investigate the mutation landscapes of inflammation-associated genes in LUAD.

Mutation Landscapes of Microbiota-Associated Inflammatory Genes in LUAD

Following our characterization of TME inflammatory profiles and bacterial compositions, we explored the genetic architecture of immune-related genes within the identified clusters. Analysis of the ImmPort dataset revealed differential expression of key inflammatory regulators: IFNGR1, CD40, and ISG15 were upregulated in Cluster 2 compared to Cluster 1, whereas BRAF, IKBKB, and IRF9 were downregulated (Figure 4A). These genes may serve as potential mechanistic links between bacterial presence and inflammatory responses in the TME. The differential expression patterns of immune-related genes, in the context of varying bacterial abundances, suggested possible genetic mechanisms underlying these associations.

We developed an interaction network between enriched bacterial species and differentially expressed immune genes, which showed that bacterial species were positively correlated with genes upregulated in Cluster 2 and negatively correlated with those downregulated (Figure 4B). This indicates a coordinated regulation of immune responses by the microbiota. Analysis of the TCGA dataset revealed that, for genes such as ISG15 exhibiting abnormal expression in over

https://doi.org/10.2147/CMAR.S520098

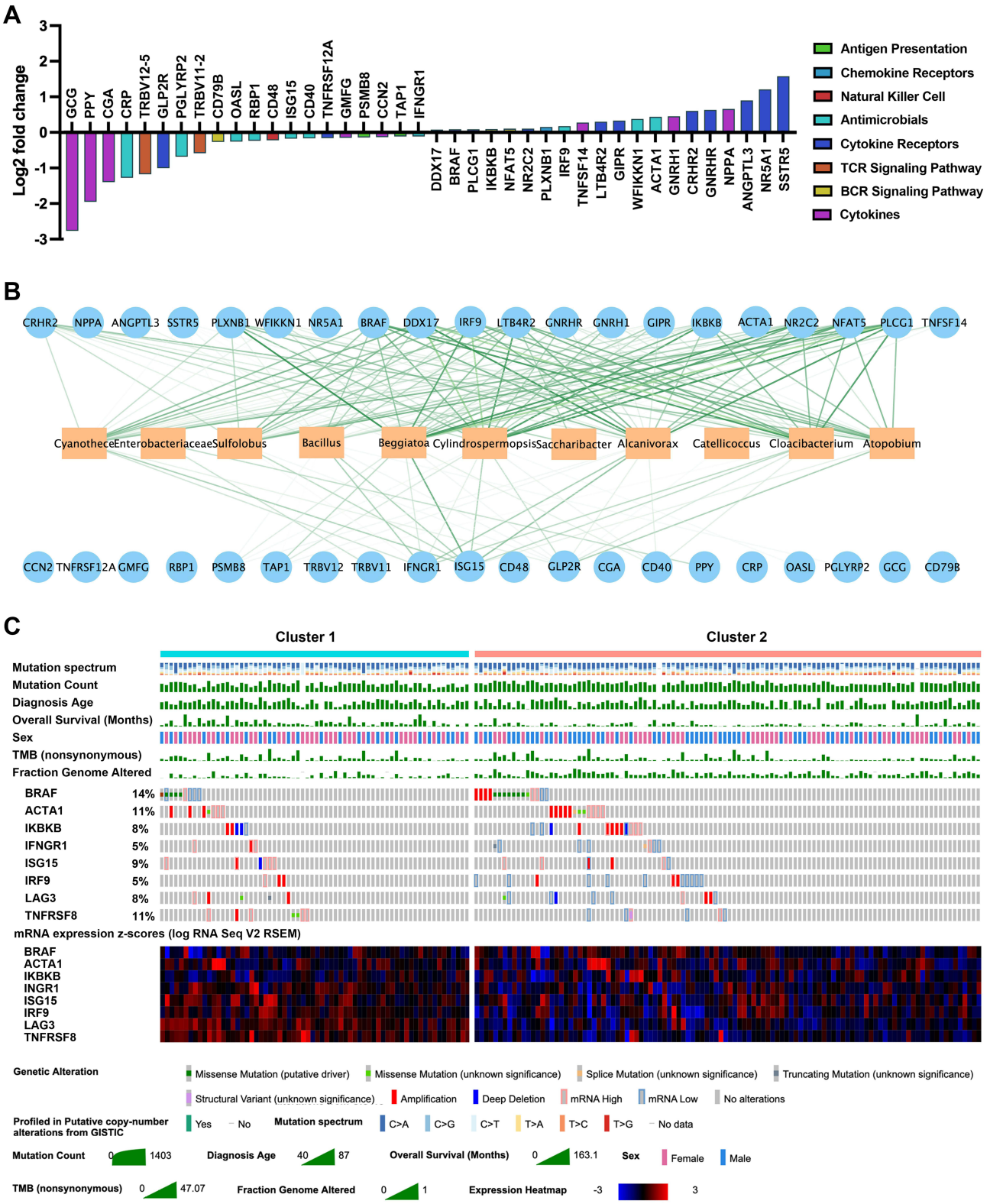

Figure 4 Microbiome-associated inflammatory gene expression and mutation profiles at varying levels of immune activation in LUAD. (**A**) Differences in expression of immune-related genes between clusters; upregulated genes are above the x-axis, downregulated genes below. Different colors represent various immune cell types. (**B**) Correlation analysis between significant commensal bacteria and differentially expressed immune-related genes. In the network diagram, rectangles represent bacteria, circles represent genes, lines indicate correlations, and line opacity reflects interaction strength (intra-group interactions not shown). (**C**) Visualization of mutations and expression profiles of immune-related genes with significant mutations across clusters using cBioPortal. The eight genes with significant mutations are indicated in the legend.

https://doi.org/10.2147/CMAR.S520098

5% of cases, these changes could not be attributed to genetic mutations (Figure 4C), suggesting that alternative regulatory mechanisms may mediate the microbiota's influence on immune gene expression.

Tumor-Associated Microbiota Influence Gene Expression and Prognosis via ceRNA Networks and Chromatin Accessibility

We extended our analysis to investigate how microbiota might regulate gene expression and affect prognosis in LUAD. Differential expression analysis identified the long non-coding RNA (lncRNA) LCIIAR as significantly upregulated in LUAD clusters ($|Log^2FC|>1$; $P<0.001$), with greater significance than other genes. Additional lncRNAs associated with the differentially expressed genes are presented in Figure 5A and Table S3. In LUAD tumor tissues, ISG15 and LCIIAR exhibited a significant positive correlation within the competing endogenous RNA (ceRNA) network ($P=7.18\times10^{-3}$) (Figure 5B and Figure S3). Spearman correlation analysis further confirmed significant associations among LCIIAR expression, ISG15 mRNA levels, and Cylindrospermopsis abundance (Figure 5C and Table S4).

Survival analyses indicated that higher expression levels of the ceRNA network genes LCIIAR and ISG15 were associated with poorer survival in LUAD patients (Figures 5D, E and S3). Using the R starBase database, we identified an lncRNA-mediated ceRNA pathway involving LCIIAR, hsa-miR-22-3p, hsa-miR-3127-5p, and ISG15 (Figure 5F). Data from the TCGA-Xena database highlighted relationships among overall survival, ISG15 gene expression, methylation, and chromatin accessibility across TCGA pan-cancer samples (Figure 5G). Tumor survival time appeared somewhat associated with ISG15 expression and chromatin accessibility in the ISG15 coding region, but not with DNA methylation in this region. Comparable data for LCIIAR are currently unavailable.

Cell Experiments Confirm the Role of LCIIAR and ISG15 in Enhancing Lung Cancer Cell Proliferation

To evaluate the effect of Cylindrospermopsis on lung adenocarcinoma cells, we co-cultured its metabolite, Cylindrospermopsin (CYN), with Lewis lung carcinoma cells. CYN reduced the expression of LCIIAR and ISG15 at low concentrations and LCIIAR expression at high concentrations (Figure 6A and B). To confirm the functional significance of LCIIAR and ISG15 in lung cancer, we conducted experiments using the Lewis lung carcinoma cell line. Transfection with siRNAs targeting LCIIAR significantly reduced its expression (Figure 6C), and siRNA-mediated knockdown of ISG15 similarly decreased its expression (Figure 6D). Furthermore, LCIIAR knockdown led to reduced ISG15 mRNA and protein levels via the ceRNA network (Figures 6E, F and S5).

Luciferase experiments demonstrated that LCIIAR increased the translation of luciferase-ISG15CDS-3'UTR, thereby enhancing ISG15 expression through post-transcriptional regulation. This effect was counteracted by miR-22-3p and miR-3127-5p mimics, while the miR-22-3p inhibitor amplified it (Figures 6G and S6). Cell proliferation assays using CCK-8 showed that altering LCIIAR and ISG15 expression significantly affected lung cancer cell proliferation, with the most pronounced effects observed 72 hours post-transfection. These results indicate that both genes play a critical role in promoting lung cancer cell proliferation (Figure 6H and I).

Discussion

In this study, we performed an in-depth analysis of microbial diversity and composition across various cancer types, focusing particularly on lung adenocarcinoma (LUAD). Our results revealed that LUAD tissues exhibit a distinct microbiota compared to other cancers, such as lung squamous cell carcinoma (LUSC), breast carcinoma (BRCA), and thyroid carcinoma (THCA). Notably, bacterial genera including Cylindrospermopsis, Cyanothece, and Sulfolobus were significantly enriched in LUAD tissues, pointing to a unique microbial signature associated with this malignancy. These findings align with growing evidence that the lung microbiome contributes to tumorigenesis and tumor progression.[9,29] By identifying significant correlations between specific bacteria, immune characteristics, and clinical outcomes in LUAD, our study expands upon this foundation.

The elevated bacterial counts and distinct microbial profiles observed in LUAD suggest that the lung microbiota exerts a substantial influence on the tumor microenvironment (TME). By clustering LUAD patients based on immunological features, we identified two groups with markedly different prognoses. Cluster 1, linked to improved survival, displayed lower bacterial

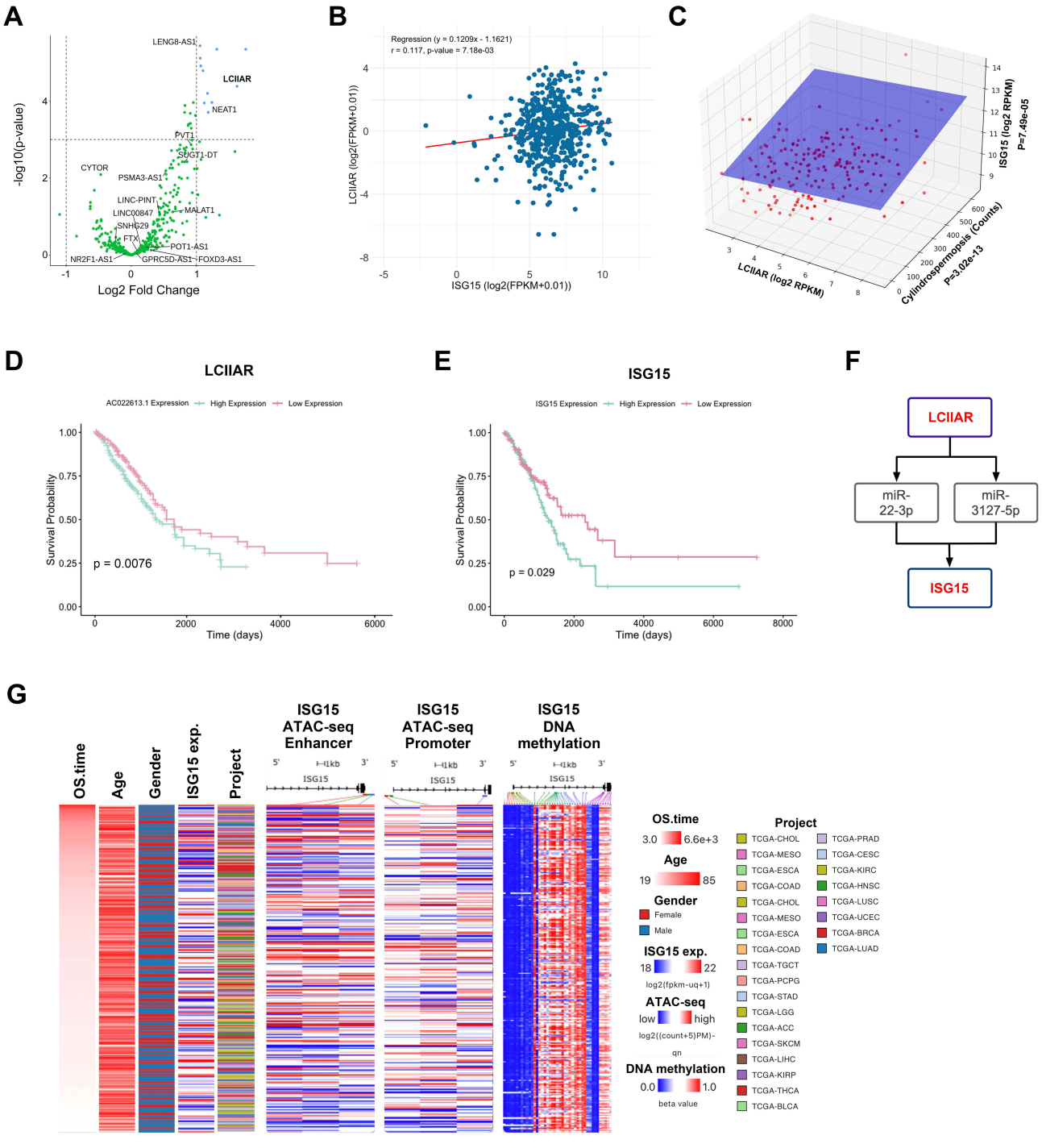

Figure 5 Tumor-associated microbiota influence gene expression and prognosis in multiple cancers through ceRNA networks and chromatin accessibility. (**A**) Volcano plot showing differential expression of lncRNA LCIIAR in LUAD clusters, with higher significance than other genes ($|Log^2FC| > 1$); $P < 0.001$ was considered statistically significant. (**B**) In LUAD tumor tissues, ISG15 and LCIIAR in the ceRNA network exhibit a significant positive correlation ($P = 7.18 \times 10^{-3}$). (**C**) Significant Spearman correlations among the expression of lncRNA LCIIAR, mRNA ISG15, and the abundance of Cylindrospermopsis. (**D**) Survival analysis showing the association between the expression of ceRNA network gene LCIIAR and LUAD patient survival. (**E**) Survival analysis showing the association between the expression of ceRNA network gene LIMD1 and LUAD patient survival. (**F**) The lncRNA-mediated ceRNA pathway (LCIIAR, hsa-miR-22-3p, hsa-miR-3127-5p, ISG15) was identified based on calculations using the R starBase database. (**G**) Visualization from the TCGA-Xena database showing the relationships among overall survival, expression and methylation, and chromatin accessibility of ISG15 in TCGA pan-cancer samples.

read counts and enrichment of genera such as Cylindrospermopsis and Saccharibacter. This cluster also exhibited robust immune responses, characterized by increased expression of MHC class I molecules, effector cells, and immune cell infiltration. Cibersortx analysis further confirmed higher proportions of effector T cells and M1 macrophages in Cluster 1, reinforcing the

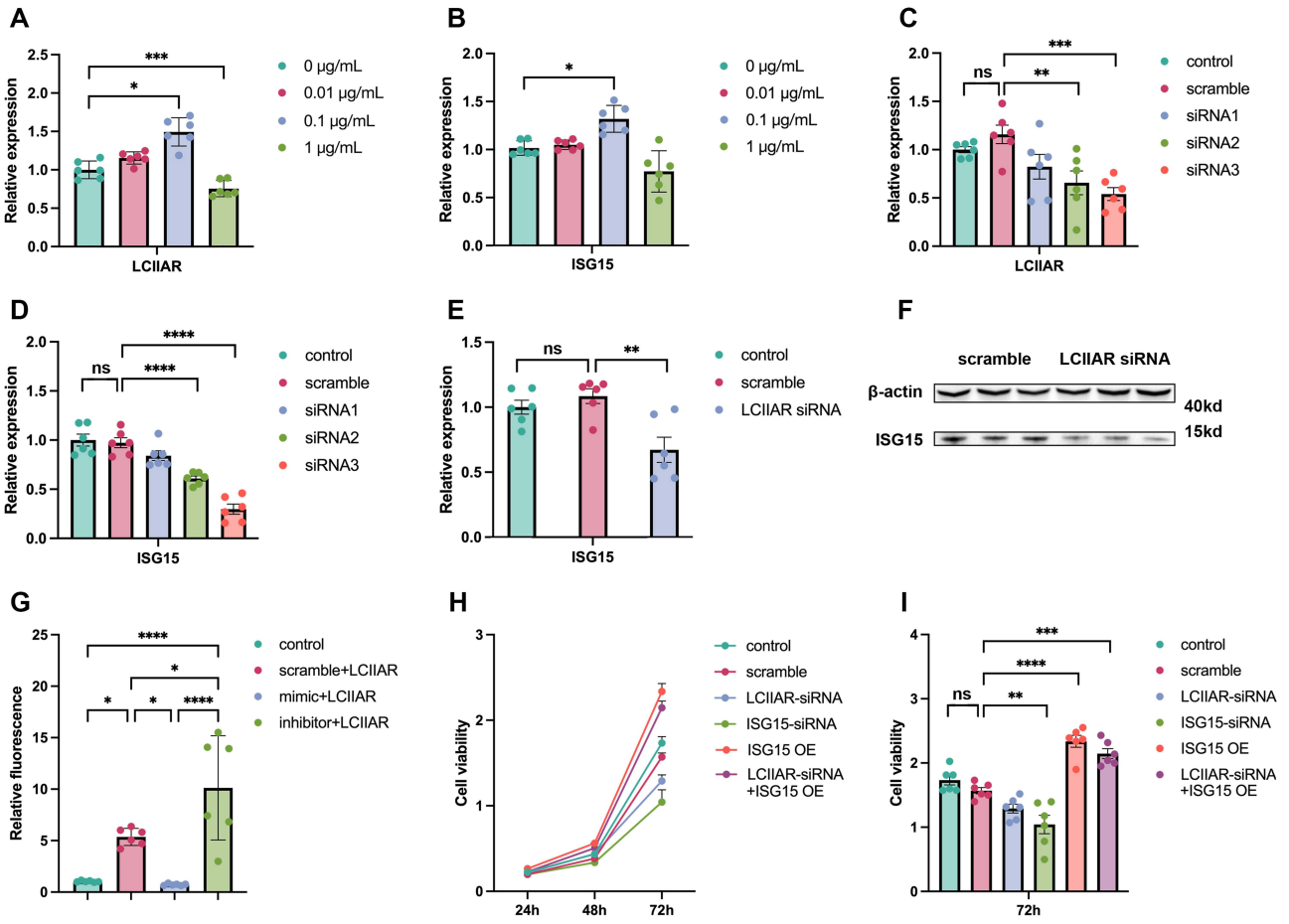

Figure 6 Cell experiments confirm that the role of bacterial metabolites and ceRNA network genes LCIIAR—ISG15 significantly influence lung cancer cell proliferation. (**A**) Cylindrospermopsin (CYN) regulates the expression of LCIIAR and (**B**) ISG15 in Lewis cell-line. (**C**) LCIIAR-siRNA reduces LCIIAR expression in Lewis cell-line. (**D**) ISG15-siRNA reduces ISG15 expression. (**E**) LCIIAR-siRNA reduces ISG15 mRNA expression via the ceRNA network in Lewis cell-line. (**F**) LCIIAR-siRNA reduces ISG15-protein expression in Lewis cell-line. (**G**) LCIIAR increases the expression level of ISG15 through post-transcriptional regulation. (**H** and **I**) CCK-8 cell proliferation assays indicate that altering the expression levels of ISG15 and LCIIAR significantly regulates the proliferation of lung cancer cell lines, with the most pronounced effect observed at 72 hours. (*$P < 0.05$, **$P < 0.01$, ***$P < 0.001$ ****$P < 0.0001$).

presence of a stronger immune response in this group. These data imply that specific commensal bacteria may foster an immune-activated TME, bolstering antitumor immunity and enhancing patient prognosis.

Our experimental findings provide deeper insight into the role of Cylindrospermopsis. We found that Cylindrospermopsin (CYN), a toxin produced by this bacterium, modulates the LCIIAR–ISG15 axis in a concentration-dependent manner. At low concentrations, CYN activates this axis and upregulates ISG15 expression, whereas at high concentrations, it suppresses ISG15 expression. Additionally, CYN exerts toxic effects on human cells, negatively regulating cell proliferation. Existing literature indicates that CYN can significantly impair lymphocyte proliferation and immune function,[30] suggesting a complex interplay with tumor proliferation and the immune microenvironment. This dual role may represent a mechanism by which Cylindrospermopsis contributes to tumor development. In contrast, current research on Cyanothece reveals no evidence of its influence on immune function. For Sulfolobus, some studies propose that it may promote immune evasion via CRISPR-Cas and CRISPR-Cmr systems, potentially enhancing tumor growth within the TME.[31,32] The increased abundance of Sulfolobus in LUAD tissues could thus contribute to an immunosuppressive microenvironment, facilitating tumor progression.

To elucidate the molecular pathways connecting the microbiota to gene expression and prognosis in LUAD, we investigated downstream mechanisms. Our analysis identified the long non-coding RNA (lncRNA) LCIIAR and the gene ISG15 as significantly upregulated in LUAD, both correlating with poorer survival. We delineated a competing endogenous RNA (ceRNA) network involving LCIIAR, hsa-miR-22-3p, hsa-miR-3127-5p, and ISG15. The positive

https://doi.org/10.2147/CMAR.S520098

correlation between LCIIAR and ISG15 expression, alongside their association with Cylindrospermopsis abundance, suggests that the microbiota may regulate gene expression through ceRNA-mediated pathways.

Cell-based experiments validated the functional roles of LCIIAR and ISG15 in driving lung cancer cell proliferation. Knockdown of LCIIAR reduced its own expression and concurrently decreased ISG15 levels via the ceRNA network. Modulating the expression of these genes significantly altered cancer cell proliferation, with the most notable effects observed 72 hours post-transfection. These findings highlight the pivotal roles of LCIIAR and ISG15 in tumor growth, positioning them as potential therapeutic targets.

Analysis of TCGA-Xena data further revealed that tumor survival time correlates to some extent with ISG15 expression and chromatin accessibility in its coding region, though not with DNA methylation in this area. Comparable epigenetic data for LCIIAR remain unavailable, marking a gap for future investigation. Together, these results illuminate the intricate regulatory networks linking the microbiota, non-coding RNAs, and epigenetic modifications in LUAD.

Our findings add to the expanding evidence base implicating the tumor microbiota in cancer development and progression. While much of the prior research has centered on the gut microbiome, particularly in colorectal cancer,[11] our study underscores the significance of the lung microbiota in LUAD. Analogous to gut microbiota–ceRNA interactions, which modulate gene expression and tumor progression,[33] our data suggest that lung microbiota exert similar effects via ceRNA networks. However, the distinct bacterial genera and molecular pathways involved reflect the unique microbial and tissue contexts of the lung, distinguishing our observations from those in gut-focused studies.

The delineation of regulatory networks involving LCIIAR and ISG15 provides novel insights into how the microbiota shapes tumor biology. These discoveries open avenues for developing diagnostic markers and therapeutic strategies targeting the lung microbiome and its associated pathways in LUAD. For example, interventions aimed at modulating the microbiota or inhibiting the LCIIAR–ISG15 axis could enhance antitumor immunity and improve clinical outcomes.

Nevertheless, our study has limitations. Although sourced from a reliable database, the microbial data may contain errors or contamination. Additionally, the observational design limits our ability to establish causality. Future studies, including in vivo models, are essential to clarify the mechanistic contributions of specific bacteria to LUAD progression.

In conclusion, our comprehensive analysis demonstrates that the tumor-associated microbiota in LUAD is intricately tied to immune characteristics, gene expression profiles, and patient prognosis. By elucidating microbial drivers and downstream molecular mechanisms, particularly the LCIIAR–ISG15 axis, this study lays the groundwork for future efforts to leverage the microbiome for therapeutic advancements in lung adenocarcinoma.

Data Sharing Statement

All raw data and code are available upon request.

Ethics Statement

This study was exempt from ethical review approval based on item 1-4 of Article 32 of the Measures for Ethical Review of Life Science and Medical Research Involving Human Subjects, dated February 18, 2023, China.

Author Contributions

Shipu Liu: data analysis; writing – original draft. Zijian Zhang: investigation; project administration; writing – review and editing. All authors made a significant contribution to the work reported, whether that is in the conception, study design, execution, acquisition of data, analysis and interpretation, or in all these areas; took part in drafting, revising or critically reviewing the article; gave final approval of the version to be published; have agreed on the journal to which the article has been submitted; and agree to be accountable for all aspects of the work.

Funding

This study was supported by the Beijing Natural Science Foundation (7242056).

Disclosure

The authors have no conflicts of interest in this work.

References

1. El Tekle G, Garrett WS. Bacteria in cancer initiation, promotion and progression. *Nat Rev Cancer*. 2023;23(9):600–618. doi:10.1038/s41568-023-00594-2
2. de Martel C, Georges D, Bray F, Ferlay J, Clifford GM. Global burden of cancer attributable to infections in 2018: a worldwide incidence analysis. *Lancet Glob Health*. 2020;8(2):e180–e190. doi:10.1016/S2214-109X(19)30488-7
3. Riquelme E, Zhang Y, Zhang L, et al. Tumor microbiome diversity and composition influence pancreatic cancer outcomes. *Cell*. 2019;178(4):795–806e12. doi:10.1016/j.cell.2019.07.008
4. Garrett WS. Cancer and the microbiota. *Science*. 2015;348(6230):80–86. doi:10.1126/science.aaa4972
5. Matson V, Fessler J, Bao R, et al. The commensal microbiome is associated with anti-PD-1 efficacy in metastatic melanoma patients. *Science*. 2018;359(6371):104–108. doi:10.1126/science.aao3290
6. Iida N, Dzutsev A, Stewart CA, et al. Commensal bacteria control cancer response to therapy by modulating the tumor microenvironment. *Science*. 2013;342(6161):967–970. doi:10.1126/science.1240527
7. Sepich-Poore GD, Zitvogel L, Straussman R, et al. The microbiome and human cancer. *Science*. 2021;371(6536). doi:10.1126/science.abc4552
8. Hong J, Guo F, Lu SY, et al. F. nucleatum targets lncRNA ENO1-IT1 to promote glycolysis and oncogenesis in colorectal cancer. *Gut*. 2021;70(11):2123–2137. doi:10.1136/gutjnl-2020-322780
9. Fidelle M, Rauber C, Alves Costa Silva C, et al. A microbiota-modulated checkpoint directs immunosuppressive intestinal T cells into cancers. *Science*. 2023;380(6649):eabo2296. doi:10.1126/science.abo2296
10. Routy B, Lenehan JG, Miller WH Jr, et al. Fecal microbiota transplantation plus anti-PD-1 immunotherapy in advanced melanoma: a Phase I trial. *Nat Med*. 2023;29(8):2121–2132. doi:10.1038/s41591-023-02453-x
11. Louis P, Hold GL, Flint HJ. The gut microbiota, bacterial metabolites and colorectal cancer. *Nat Rev Microbiol*. 2014;12(10):661–672. doi:10.1038/nrmicro3344
12. Dickson RP, Erb-Downward JR, Martinez FJ, et al. The microbiome and the respiratory tract. *Annu Rev Physiol*. 2016;78:481–504. doi:10.1146/annurev-physiol-021115-105238
13. Tsay JJ, Wu BG, Badri MH, et al. Airway microbiota is associated with upregulation of the PI3K pathway in lung cancer. *Am J Respir Crit Care Med*. 2018;198(9):1188–1198. doi:10.1164/rccm.201710-2118OC
14. Nicholson AG, Tsao MS, Beasley MB, et al. The 2021 WHO classification of lung tumors: impact of advances since 2015. *J Thorac Oncol*. 2022;17(3):362–387. doi:10.1016/j.jtho.2021.11.003
15. Jin C, Lagoudas GK, Zhao C, et al. Commensal microbiota promote lung cancer development via gammadelta T cells. *Cell*. 2019;176(5):998–1013e16. doi:10.1016/j.cell.2018.12.040
16. Segal LN, Alekseyenko AV, Clemente JC, et al. Enrichment of lung microbiome with supraglottic taxa is associated with increased pulmonary inflammation. *Microbiome*. 2013;1(1):19. doi:10.1186/2049-2618-1-19
17. Poore GD, Kopylova E, Zhu Q, et al. Microbiome analyses of blood and tissues suggest cancer diagnostic approach. *Nature*. 2020;579(7800):567–574. doi:10.1038/s41586-020-2095-1
18. Bagaev A, Kotlov N, Nomie K, et al. Conserved pan-cancer microenvironment subtypes predict response to immunotherapy. *Cancer Cell*. 2021;39(6):845–65e7. doi:10.1016/j.ccell.2021.04.014
19. Cao S, Wendl MC, Wyczalkowski MA, et al. Divergent viral presentation among human tumors and adjacent normal tissues. *Sci Rep*. 2016;6:28294. doi:10.1038/srep28294
20. Dixon P. VEGAN, a package of R functions for community ecology. *J Veg Sci*. 2003;14(6):927–930. doi:10.1111/j.1654-1103.2003.tb02228.x
21. Podani J, Miklós I. Resemblance coefficients and the horseshoe effect in principal coordinates analysis. *Ecology*. 2002;83(12):3331–3343. doi:10.1890/0012-9658(2002)083[3331:Rcathe]2.0.Co;2
22. Love MI, Huber W, Anders S. Moderated estimation of fold change and dispersion for RNA-seq data with DESeq2. *Genome Biol*. 2014;15(12). doi:10.1186/s13059-014-0550-8
23. Gaujoux R, Seoighe C. A flexible R package for nonnegative matrix factorization. *BMC Bioinf*. 2010;11:367. doi:10.1186/1471-2105-11-367
24. von Mering C, Huynen M, Jaeggi D, et al. STRING: a database of predicted functional associations between proteins. *Nucleic Acids Res*. 2003;31(1):258–261. doi:10.1093/nar/gkg034
25. Bader GD, Hogue CW. An automated method for finding molecular complexes in large protein interaction networks. *BMC Bioinf*. 2003;4:2. doi:10.1186/1471-2105-4-2
26. Saito R, Smoot ME, Ono K, et al. A travel guide to Cytoscape plugins. *Nat Methods*. 2012;9(11):1069–1076. doi:10.1038/nmeth.2212
27. Li R, Qu H, Wang S, et al. GDCRNATools: an R/Bioconductor package for integrative analysis of lncRNA, miRNA and mRNA data in GDC. *Bioinformatics*. 2018;34(14):2515–2517. doi:10.1093/bioinformatics/bty124
28. Wang P, Guo Q, Hao Y, et al. LnCeCell: a comprehensive database of predicted lncRNA-associated ceRNA networks at single-cell resolution. *Nucleic Acids Res*. 2021;49(D1):D125–D33. doi:10.1093/nar/gkaa1017
29. Goto T. Microbiota and lung cancer. *Semin Cancer Biol*. 2022;86(Pt 3):1–10. doi:10.1016/j.semcancer.2022.07.006
30. Casas-Rodríguez A, Cebadero-Dominguez Ó, Puerto M, et al. Immunomodulatory effects of cylindrospermopsin in human T cells and monocytes. *Toxins*. 2023;15(4):301. doi:10.3390/toxins15040301
31. Zhang J, Rouillon C, Kerou M, et al. Structure and mechanism of the CMR complex for CRISPR-mediated antiviral immunity. *Mol Cell*. 2012;45(3):303–313. doi:10.1016/j.molcel.2011.12.013
32. Pauly MD, Bautista MA, Black JA, et al. Diversified local CRISPR-Cas immunity to viruses of Sulfolobus islandicus. *Philos Trans R Soc Lond B Biol Sci*. 2019;374(1772):20180093. doi:10.1098/rstb.2018.0093
33. Zhao LY, Mei JX, Yu G, et al. Role of the gut microbiota in anticancer therapy: from molecular mechanisms to clinical applications. *Signal Transduct Target Ther*. 2023;8(1):201. doi:10.1038/s41392-023-01406-7